Impact of using dual back surface field layers of different materials on GaAs single junction solar cell performance

Ala'eddin A. Saif*, A. Mindil
Department of Physical Science, College of Science, University of Jeddah, Jeddah, Saudi Arabia

This research aspires to investigate the impact of employing dual BSF layers on the performance of single junction GaAs solar cells using the Silvaco TCAD simulator. A layer of GaAs, InGaP, and InAlGaP has been implemented as a second BSF layer on top of the original BSF layer of the n-InGaP/n-GaAs/p-GaAs/p-InAlGaP structured solar cell. The results show that using GaAs as a second BSF layer has increased the carrier's recombination and degraded the cell efficiency due to its lower energy bandgap, which creates a potential well that lessens the number of photogenerated carriers flowing through the conduction band toward electrodes. However, adding InGaP and InAlGaP as a second BSF layer decreases the recombination rate and generates a broad electric field region leading to extra photogenerated carriers drifting through the cell, which increases the efficiency from 29.42% to 29.81% for the case of using InGaP and 30.33% for the case of using InAlGaP. Furthermore, increasing the thickness and doping of the second BSF layer reduces the carriers' recombination at the boundaries of this layer, which implies efficiency enhancement.

(Received March 25, 2024; Accepted August 13, 2024)

Keywords: GaAs single junction, Solar cell, Dual BSF layers, Efficiency, Silvaco

1. Introduction

There is increasing concern about renewable energy sources, especially solar energy, due to their practical impact on reducing environmental pollution and global warming from fossil fuels and oil [1-3]. This motivates many researchers to find new materials to be used as the active region where most of the photoabsorption and electron-hole pairs generation occurs in photovoltaic cells. Besides, proposing different cell structure designs that give high conversion efficiency [4-6]. One of the most effective and widely studied materials for single-junction and multi-junction solar cells is GaAs due to the reasonable energy bandgap of 1.42 eV, which allows absorbing a long range of wavelengths of the visible spectrum of solar radiation [7, 8]. The single junction solar cells suffer from high recombination for the photogenerated carrier on the surfaces due to defects or contamination that can trap charge carriers at interfaces, causing them to recombine rather than participate in the current flow, consequently degrading the solar cell efficiency. Thus, many researchers propose to include a front surface field (FSF) layer and back surface layer (BSF) that must have a higher energy bandgap than the active material bandgap. These layers would minimize the recombination of carriers at the cell's surfaces and enhance the output photocurrent [9, 10].

In previous research, a GaAs solar cell with InGaP as the FSF layer and InAlGaP as the BSF layer is proposed to find out that the efficiency has been improved and reaches up to 30.88% [11]. Other researchers reported more studies for improving the GaAs solar cells' photovoltaic properties using different couples of materials representing the FSF and BSF layers [12-16]. In the current work, a second back surface field layer is proposed to be sandwiched between the original BSF layer and the base of n-InGaP/n-GaAs/p-GaAs/p-InAlGaP single junction solar cell to investigate its impact on its performance. Three materials, namely: GaAs, InGaP, and InAlGaP, have been tested as a second back surface field layer, and their effect on the solar cell performance is deeply investigated and compared.

* Corresponding author: aasaif@uj.edu.sa
https://doi.org/10.15251/JOR.2024.204.569

2. Solar cells structure and simulation

In this research, a single-junction GaAs solar cell structure using the layers' doping concentrations and thicknesses, shown in Figure 1(a), is proposed. This structure is investigated by implementing a second BSF on top of the original one, as shown in Figure 1(b). The thickness of the new BSF layer is 0.05 µm, and the doping concentration used is 1×10^{19} cm^{-3}. Three materials have been used to represent the second BSF layer: GaAs, InGaP, and InGaAlP. The selection of these materials is based on the equality of the lattice constant to avoid interface mismatching as much as possible, in addition, they are already used for the original solar cell. The simulation conditions regarding physical models and materials parameters are the same as in the previous work [11]. To study the properties of the proposed solar cell model, it is illuminated using the AM1.5G spectrum, shown in Figure 2.

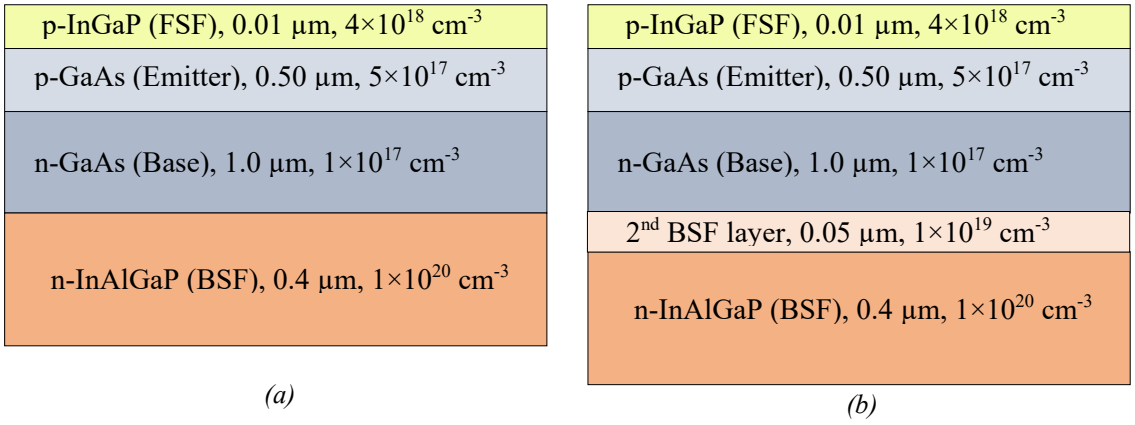

Fig. 1. GaAs solar cell of (a) a single BSF layer and (b) dual BSF layers.

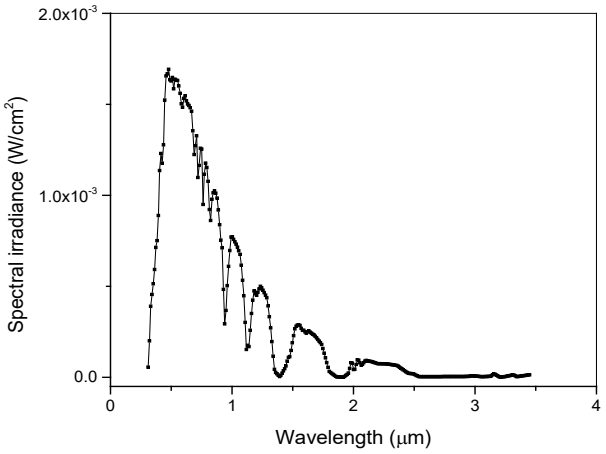

Fig. 2. AM1.5G spectrum used to illuminate the solar cell.

3. Results and discussion

In order to examine the impact of the second BSF layer of different materials, the J-V curve for the solar cell of dual BSF layers and the one with only a single BSF layer are extracted and plotted, as shown in Figure 3. The values of short circuit current (I_{sc}), Open circuit voltage (V_{oc}), maximum power (P_m), fill factor (FF), and efficiency (η) parameters are evaluated and tabulated in Table 1. It is noticed that the solar cell that included GaAs as the second BSF layer shows a degradation in its performance compared to the solar cell with a single BSF layer. On the other hand, the solar cells that contain InGaP and InAlGaP as the second BSF layer show a noticeable

improvement in their performance, where their efficiency rises from 29.42% for the cell of single BSF layer to 29.81% and 30.33% for the cells with InGaP and InAlGaP as a second BSF layer, respectively.

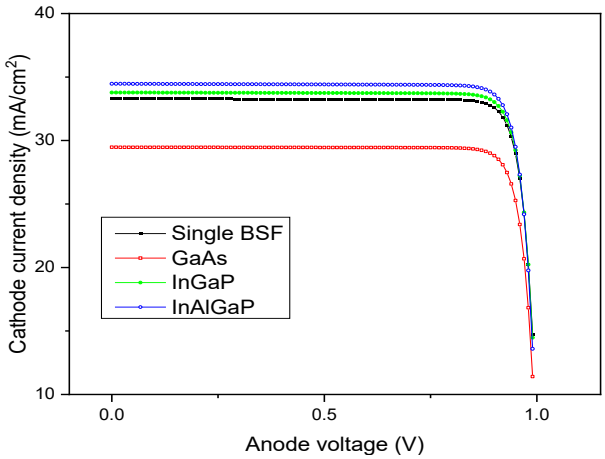

Fig. 3. J-V curve of the single junction GaAs solar cell with a single BSF layer and the solar cells with GaAs, InGaP, and InAlGaP as the second BSF layer.

Table 1. Solar cells' parameters.

Sample	I_{sc} (mA/cm^2)	V_{oc} (V)	P_m (mW/cm^2)	FF (%)	η (%)
Single BSF	33.29	1.007	29.38	87.66	29.42
GaAs	29.47	1.004	25.95	87.72	25.98
InGaP	33.78	1.006	29.77	87.61	29.81
InAlGaP	34.47	1.004	30.29	87.48	30.33

To understand the influence of implementing the second BSF layer into GaAs solar cells, the cutline of the recombination rate along the cells under investigation is plotted versus the solar cell depth, as shown in Figure 4. The figure shows that the recombination rate in the top layers of solar cells, i.e., FSF, emitter, and base layers is almost unchanged. However, an increase in the recombination for the solar cell containing GaAs as the second BSF layer is noticed within the BSF layers, which explains the reduction in the conversion efficiency as compared to the solar cell with a single BSF layer. In contrast, the solar cells that possess InGaP and InAlGaP as the second BSF layer show a lowering in the recombination rate within the BSF. This implies that the photogenerated charges have a greater lifetime; thus, they can be collected at the electrodes before recombining; as a result, the performance of the solar cells is enhanced.

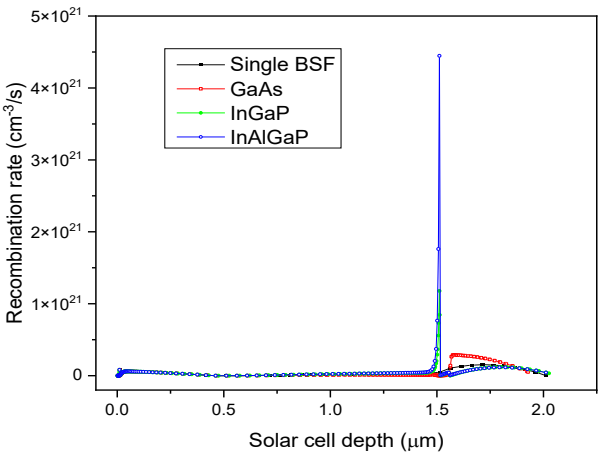

Fig. 4. Cutline of recombination rate of the single junction GaAs solar cell with a single BSF layer and the solar cells with GaAs, InGaP, and InAlGaP as the second BSF layer.

The energy band diagram for the solar cells under testing is plotted along their depth, as shown in Figure 5. It is observed that the solar cell that has GaAs as the second BSF layer shows a potential well within the conduction band between the base and original BSF layer, as depicted in Figure 5(b). This is due to the lower energy bandgap of GaAs BSF of 1.42 eV compared to the original InAlGaP BSF layer of 2.4 eV. This implies that the photogenerated electrons, after dropping inside this potential well while drifting along the conduction band, suffer a potential step that hardens their flow toward the contact and minimizes the number of collected photogenerated electrons; as a result, a lower conversion efficiency compared to the single BSF solar cell is obtained. The solar cells that consist of InGaP and InAlGaP as the second BSF layer show a lowering potential step within the bands, as shown in Figures 5(c) and 5(d); this potential step fastens the photogenerated carriers to accelerate toward contacts. This explains their higher efficiency compared to the single BSF solar cell.

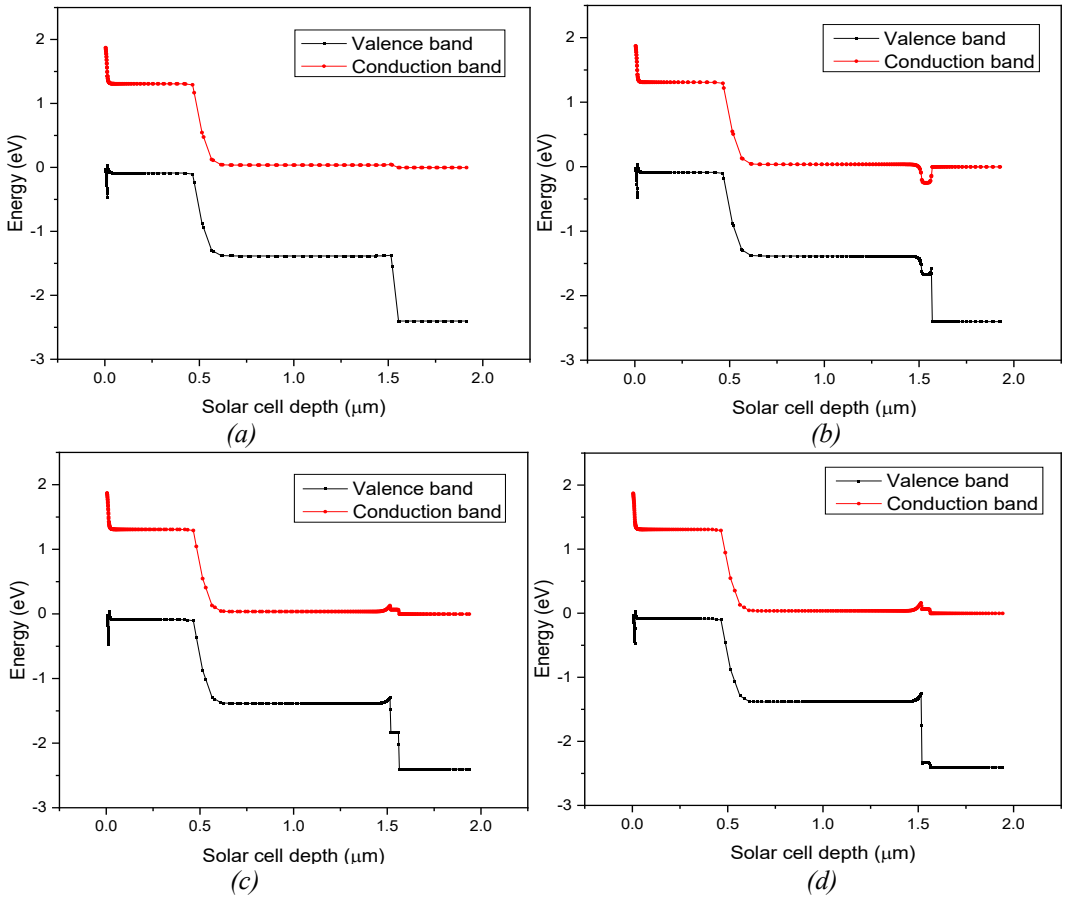

Fig. 5. Energy bandgap diagram of (a) GaAs solar cell with a single BSF layer and solar cells with (b) GaAs, (c) InGaP, and (d) InAlGaP as the second BSF layer.

In order to have further insight into the impact of implementing the second BSF layer into GaAs solar cells, the cutline of the electric field along the cells is plotted in Figure 6. It is noticed that for the solar cell with a single BSF layer, a tiny electric field peak is created at the BSF-base boundary, as illustrated in Figure 6(a). This electric field is typically formed due to the BSF layer; it aids in electron-hole separation and pushes them toward electrodes to contribute to the total current [17, 18]. However, two peaks for the solar cells with dual BSF layers are observed. The first one is within the region between the second BSF layer and base, and the second peak is between the BSF layers. These peaks are created due to the doping gradient between the second BSF layer and the adjacent layers, which generate junctions between these layers, forming built-in electric fields [19, 20].

In the cell that contains GaAs as the second BSF layer, the electric field peaks are pretty high and sharp, with a relatively stronger peak between the BSF layers, as depicted in Figure 6(b). The sharpness of the electric field peaks indicates that these fields are produced within a narrow width between layers; thus, their effect on drifting the photogenerated carriers would be in short range. Furthermore, due to the closeness of these two electric field peaks, their impact on carriers drifting would be opposed, which means there is a high probability of recombination of the carriers within the region between the field regions. This explains the increase of the recombination rate for the cell having GaAs as the second BSF layer, as discussed in Figure 4. At the same time, it explains the degradation in the conversion efficiency in this solar cell.

On the other hand, the solar cells that possess InGaP and InAlGaP as the second BSF layer show a much broader electric field peak between the second BSF layer and the base compared to the one created between the BSF layers, as illustrated in Figures 6(c) and 6(d), respectively. The wideness of the field peak between the second BSF layer and the base indicates that its effect would be extended for a longer range to the other peak. This means that its impact on photogenerated carriers drifting will be dominant; subsequently, less chance of carriers' recombination between the two built-in field regions is expected compared to the cell with GaAs as the second BSF layer. The strong and wide range electric field between the second BSF and the base regions would greatly impact delivering a larger number of charged carriers to the contacts, thus increasing the efficiency of these cells.

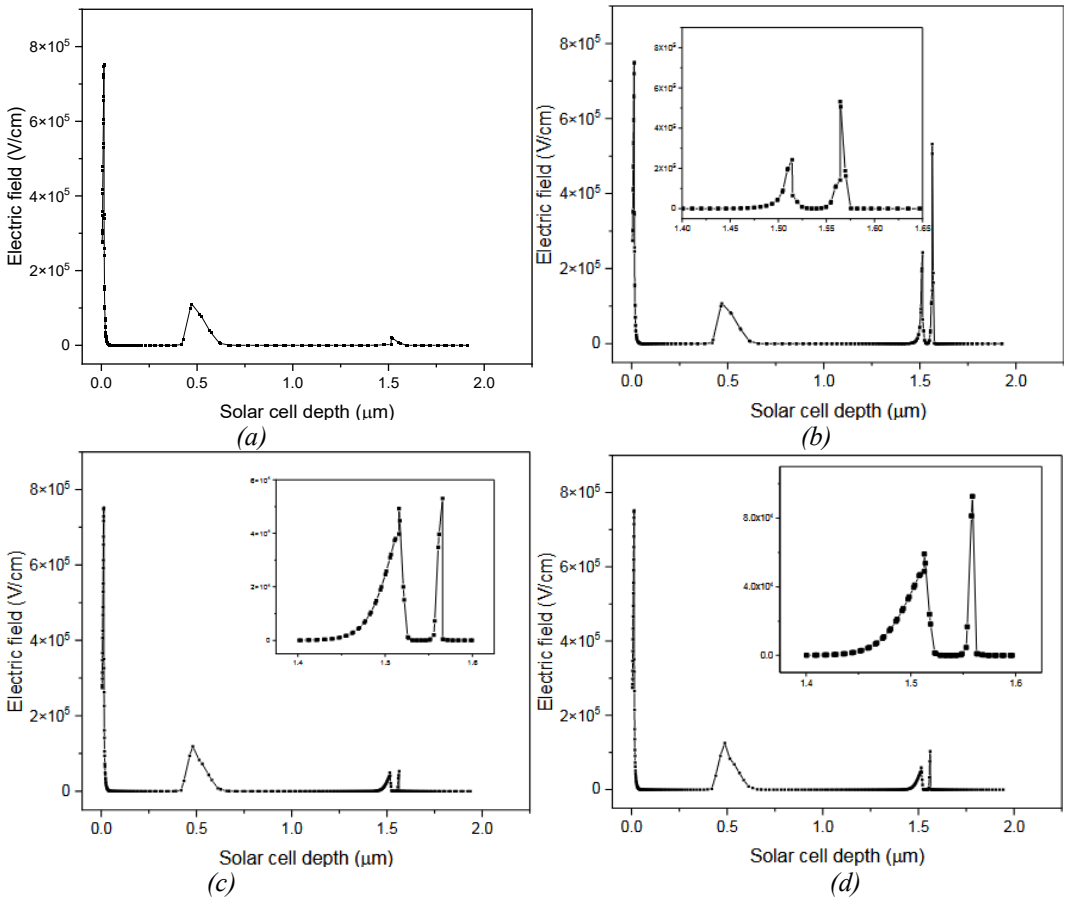

Fig. 6. Electric field cutline of (a) GaAs solar cell with a single BSF layer and solar cells with (b) GaAs, (c) InGaP, and (d) InAlGaP as the second BSF layer.

For further information about the influence of using the second BSF layer on solar cell efficiency, the impact of its thickness and doping on efficiency have been studied and plotted, as

shown in Figure 7. In this context, InAlGaP as a second BSF layer in the solar cell is discussed. The second BSF layer's thickness varies from 0.01 µm to 0.09 µm at a fixed doping level. The results show that the efficiency is almost linearly increased with the thickness, as depicted in Figure 7(a), which could be correlated to the increment of collected photogenerated carriers within the BSF layer that contributes to the total photocurrent [22]. The doping of the second BSF layer is studied in the range of 1×10^{15} cm^{-3} to 1×10^{21} cm^{-3}, as shown in Figure 7(b). The results show that the efficiency increases with the doping level up to 30.37% at doping of 1×10^{20} cm^{-3} then decreases at higher doping. The increase in the efficiency of the solar cell with doping is attributed to the decrement in the carriers' recombination [23]. Further analysis of the second BSF layer's doping influence on charge recombination will be discussed in Figure 10.

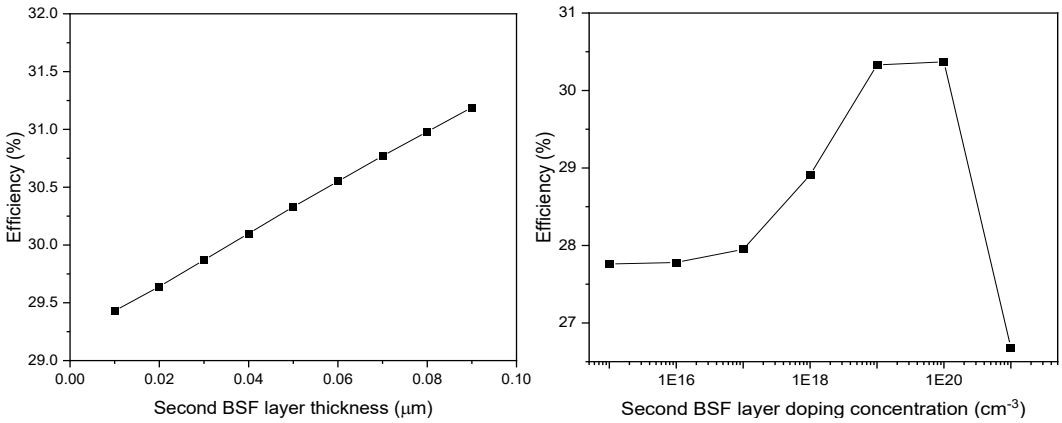

(a) *(b)*

Fig. 7. Variation of GaAs solar cell efficiency with the (a) thickness and (b) doping concentration of the second InAlGaP BSF layer.

The variation in the recombination rate along the depth of the solar cell for different thicknesses of the second InAlGaP BSF layer is plotted in Figure 8. It has been noted that as the thickness of the second InAlGaP BSF layer increases, the recombination peak at the interface between the second BSF layer and the base decreases. This suggests that the efficiency of the solar cell is improved. The reduction in the carriers' recombination can be explained as follows: increasing the thickness of the second BSF layer leads to moving the back surface further away from the active region, which reduces the surface recombination velocity [24]. Additionally, increasing the second BSF layer thickness at fixed doping implies that the charged carriers would have fewer chances to encounter impurity defects, resulting in a decrement in carriers' recombination.

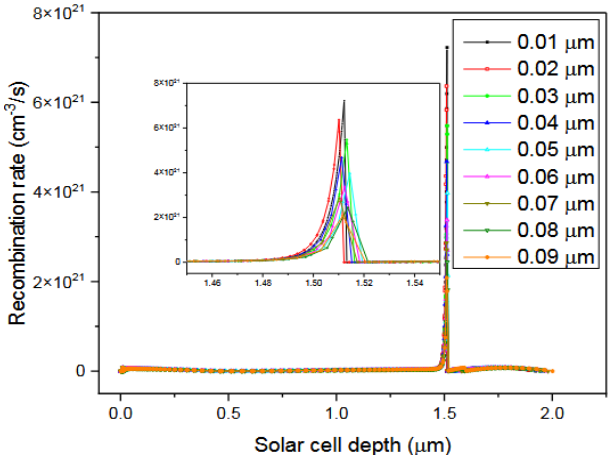

Fig. 8. Cutline of the recombination rate along the GaAs solar cell with InAlGaP as the second BSF layer at different thicknesses.

The cutline of the electric field along the solar cell with InAlGaP as the second BSF layer at different thicknesses is plotted in Figure 9. It is noted that the electric field peak at the boundary between the second BSF layer and the base is widened with the increase of the second BSF layer thickness due to the depletion region widening because of the doping gradient. The strength of the electric field between the BSF layers reduces with the thickness. As the second BSF layer thickness increases, the distance between the BSF layers increases; subsequently, the distance between the electric field region becomes farther. Thus, the potential generated between the BSF layers would have a weak gradient to build up more charges at the second BSF layer; therefore, the electric field strength between BSF layers is weakened.

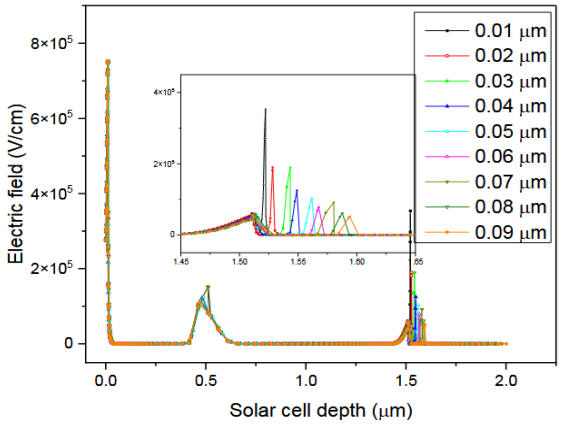

Fig. 9. Cutline of the electric field along the GaAs solar cell with InAlGaP as the second BSF layer at different thicknesses.

The variation of the recombination rate as a function of the solar cell depth at various doping concentrations of the second InAlGaP BSF layer is illustrated in Figure 10. From inset A in Figure 10, it is noticed that the intensity of the recombination peak created at the boundary between the second BSF layer and the base region decreases with the doping increase. To get a deeper view of the effect of doping on carriers' recombination within the second BSF layer, the recombination rate plot is zoomed in to this layer as depicted in inset B in Figure 10. A tinny recombination peak is noticed within the second InAlGaP BSF layer; its intensity is degraded with the doping increment within this layer. The decrement in the carriers' recombination as the doping increases explains the efficiency increment at these doping concentrations, as discussed in Figure 7(b).

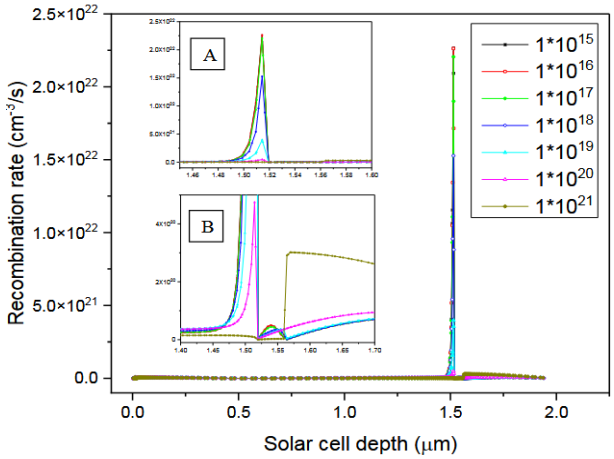

Fig. 10. Cutline of the recombination rate along the GaAs solar cell with InAlGaP as the second BSF layer at different doping concentration.

The electric field variation along the solar cell with InAlGaP as the second BSF layer at different doping concentrations is plotted as shown in Figure 11. It is noticed that the strength of the electric field at the boundaries of the second BSF layer decreases as the doping concentration increases. The decrement in the electric field can be explained as follows: as the doping of the second BSF layer increases, the dopant atoms become more closely packed within this layer. This likely causes frequent collisions between charged carriers and impurities. Thus, the mobility of the carriers is reduced [25], which limits their ability to contribute to the overall electric field, as a result, the electric field strength decreases. Interestingly, the recombination peak between the BSF layers at doping of 1×10^{20} cm^{-3} disappeared due to their equality in their doping level.

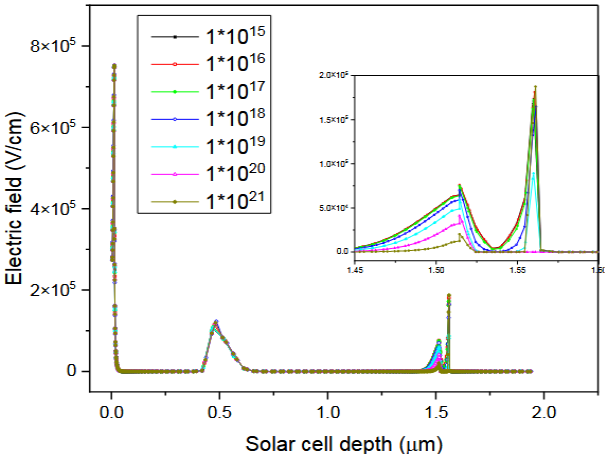

Fig. 11. Cutline of the electric field along the GaAs solar cell with InAlGaP as the second BSF layer at different doping concentration.

4. Conclusion

The impact of implementing dual back surface field layers within n-InGaP/n-GaAs/p-GaAs/p-InAlGaP configured solar cell on its performance has been analyzed with the aid of the Silvaco simulator. The materials used as the second back surface field layer are the same for the proposed cell, i.e., GaAs, InGaP, and InAlGaP. It is found that using GaAs lowers the efficiency from 29.42% to 25.98%, which is attributed to its narrower energy bandgap compared to the InAlGaP. The bandgap gradient produces a potential well that acts as a trap for photogenerated electrons while flowing through the conduction band toward electrodes. On the contrary, adding InGaP and InAlGaP as a second BSF layer increases the cell efficiency from 29.42% to 29.81% and to 30.33% for the cases of using InGaP and InAlGaP as the second BSF layer, respectively. The improvement in the efficiency of these cells is correlated to the lowering potential step that helps to drift the photogenerated carriers toward contacts. Besides, generating a broad electric field region between the base and original BSF layers caused further photogenerated carriers to contribute to the total photocurrent. The efficiency of the solar cell shows an increment with the increase in the thickness and doping concentration of the second InAlGaP BSF layer, which is correlated to the reduction of the carriers' recombination within the BSF layer.

Acknowledgments

This work was funded by the University of Jeddah, Jeddah, Saudi Arabia, under grant No. (UJ-24-DR-4220589-1). The authors, therefore, thank the University of Jeddah for its technical and financial support.

References

[1] A. Jangjoy, H. Bahador, H. A. Heidarzadeh, Plasmonics, **16**, 395–401 (2021); https://doi.org/10.1007/s11468-020-01297-2
[2] Y. Meng, L. Yanqiu, Ch. Qijin, L. Shuai, Solar Energy, **182**, 453-461 (2019); https://doi.org/10.1016/j.solener.2019.02.061
[3] A. Imran, M. Sulaman, Y. Song, D. Eric, M. N. Zahid, M. Yousaf, M.I. Saleem, M. Li, D. Li, M Journal of Computational Electronics, **20**, 310–316 (2021); https://doi.org/10.1007/s10825-020-01583-6
[4] K. Sidra, K. Y. Satish, S. Jyotsna, B. S. Rajendra, Heliyon, **8**, e09941 (2022); https://doi.org/10.1016/j.heliyon.2022.e09941
[5] I. M. Alarifi, Material Today: Proceedings, **81**, 403-414, (2023); https://doi.org/10.1016/j.matpr.2021.03.427
[6] H. Soonmin, Hardani, P. Nandi, B.S. Mwankemwa, T.D. Malevu, M.I. Malik, Applied Sciences, **13**, 2051, (2023); https://doi.org/10.3390/app13042051
[7] X. Yu, Y. Dai, Y. Lu, C. Liu, Y. Yan, R. Shen, Z. Yang, L. Feng, L. Sun, Y. Liu, S. Lin, Advanced Science, **10**, 2204058 (2023); https://doi.org/10.1002/advs.202204058
[8] G. S. Sahoo, G. P. Mishra, Efficient Journal of Electronic Materials, **48**, 560–570 (2019). https://doi.org/10.1007/s11664-018-6743-2
[9] H. V. D. John, D. J. Moni, D. Gracia, Przegląd Elektrotechniczny, **12**, 9-18 (2020). http://dx.doi.org/10.15199/48.2020.12.02.
[10] C. F. Kamdem, A.T. Ngoupo, F.K. Konan, H.J. Nkuissi, B. Hartiti, J. Ndjaka, Indian Journal of Science and Technology, **12**, 1-9 (2019). https://dx.doi.org/10.17485/ijst/2019/v12i37/147207
[11] A. A. Saif, Results in Optics, **12**, 100454 (2023); https://doi.org/10.1016/j.rio.2023.100454
[12] M. Gamel, K.P. Jern, E. Rashid, L. H. Jing, L.K. Yao, B. Wong, E IEEE International Conference on Sensors and Nanotechnology, 1-4 (2019); https://doi.org/10.1109/SENSORSNANO44414.2019.8940098.
[13] C. Palacios, N. Guerra, M. Guevara, M. López, Revista de I+D Tecnológico 14, 96 (2018); https://doi.org/10.33412/idt.v14.2.2078
[14] M. Abderrezek, F. Djahli, M. Fathi, M. Ayad, Elektronika Ir Elektrotechnika, **19**, 41 (2013). https://doi.org/10.5755/j01.eee.19.8.5392
[15] K. Attari, L. Amhaimar, A. El yaakoubi, A. Asselman, M. Bassou, International Journal of Photoenergy, **2017**, 8269358(2017). https://doi.org/10.1155/2017/8269358.
[16] A. A. Saif, M. Albishri, A. Mindil, M. Qaeed, Journal of Ovonic Research, **19**, 1–14 (2023). https://doi.org/10.15251/JOR.2023.191.1
[17] K.S. Choe, Solid State Sciences, **29**, 48-51 (2014); https://doi.org/10.1016/j.solidstatesciences.2014.01.005.
[18] K. Ali, Z. Ali, Solar Energy, **225**, 91-96 (2021); https://doi.org/10.1016/j.solener.2021.07.027
[19] Y.J. Zhao, S. Li, H.X. Ren, S.J. Li, P.D. Han, Journal of Semiconductors, **42**, 032701 (2021); https://doi.org/10.1088/1674-4926/42/3/032701
[20] X. Qin, Q. Shi, F. Shi, Y. Li, D. Song, Advances in Multimedia, **2022**, 5157252 (2022); https://doi.org/10.1155/2022/5157252
[21] H. R. Devi, O.Y. Bisen, S. Nanda, R. Nandan, K. K. Nanda, Current Science, **121**, 894-898 (2021); https://doi.org/10.18520/cs/v121/i7/894-898
[22] M. S. Rana, M. M. Islam, M. Julkarnain, Solar Energy, **226**, 272–287, (2021); https://doi.org/10.1016/j.solener.2021.08.035
[23] A. Talhi, M. Boukais, B. Dennai, A. Ouldabbes, Journal of Ovonic Research, **15**, 157-160 (2019).
[24] S. Gatz, J. Müller, T. Dullweber, R. Brendel, Energy Procedia, **27**, 95-102 (2012); https://doi.org/10.1016/j.egypro.2012.07.035
[25] C. F. Kamdem, A. T. Ngoupo, F. X. A. Abega, A. M. N. Abena, J.B. Ndjaka, International Journal of Photoenergy, **2023**, 6204891 (2023); https://doi.org/10.1155/2023/6204891